Michigan State University

National Superconducting Cyclotron Laboratory

NUCLEAR DISASSEMBLY IN SYMMETRIC HEAVY-ION COLLISIONS AT INTERMEDIATE ENERGIES.♠

W. J. LLOPE and the MSU 4π Group:

National Superconducting Cyclotron Laboratory, Michigan State University;

Dept. of Chemistry, State University of New York - Stony Brook;

Dept. of Physics, University of Michigan - Dearborn;

Cyclotron Institute, Texas A&M University;

Dept. of Physics, University of Iowa.

♠Talk given at the 10th Winter Workshop on Nuclear Dynamics, Snowbird, Utah (Jan. 15-21, 1994).

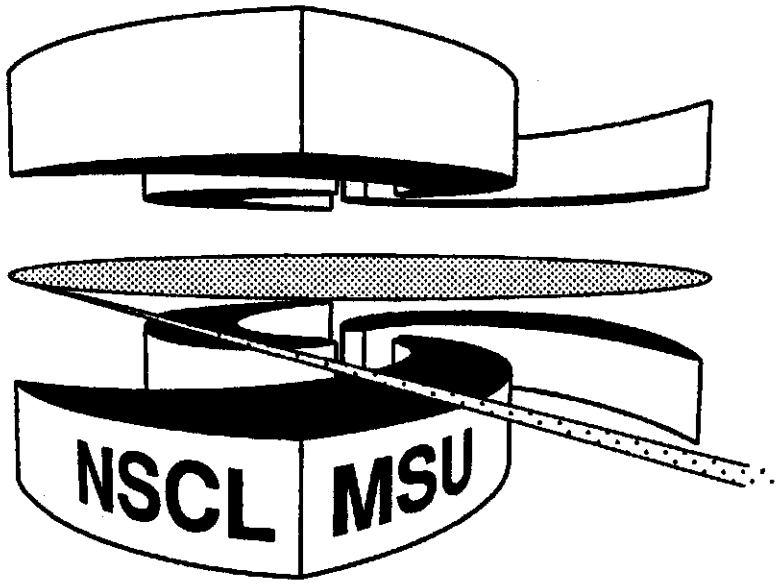

MSUCL-915 **January 1994**

NUCLEAR DISASSEMBLY IN SYMMETRIC HEAVY-ION COLLISIONS AT INTERMEDIATE BEAM ENERGIES.+

W. J. LLOPE and the MSU 4π GROUP§
National Superconducting Cyclotron Laboratory
Michigan State University
East Lansing, MI 48824-1321, USA

ABSTRACT

We have experimentally studied small impact parameter heavy-ion collisions in the (nearly) symmetric entrance channels $^{12}C+^{12}C$, $^{20}Ne+^{27}Al$, $^{40}Ar+^{45}Sc$, $^{84}Kr+^{93}Nb$, and $^{129}Xe+^{139}La$, each at many intermediate beam energies. Several analysis strategies based on the "shapes" of the experimental events are used toinvestigate the relative efficiencies of various experimental methods for the selection of the most central collisions, and to search for possible beam energy-dependent transitions from sequential binary disassembly to multifragmentation in the central events. Comparisons to dynamical and hybrid model code calculations will be discussed. The average shapes of subsets of the central events, in particular the intermediate mass fragments (IMFs, for which $3 \lesssim Z \lesssim 20$), are presented. Critical behavior, attributed to a transition from sequential binary disassembly to multifragmentation, is observed in all of these analyses. The transitional beam energies for the central $^{40}Ar+^{45}Sc$, $^{84}Kr+^{93}Nb$, and $^{129}Xe+^{139}La$ reactions are near -55, -40, and -40 MeV/nucleon, respectively.

1. Introduction

It is possible to form excited nuclear systems in the laboratory by colliding atomic nuclei. The impact parameter, as well as the predominant reaction mechanisms at each impact parameter, can be inferred from the experimentally measured characteristics of the particle emission. Given an efficient experimental selection of the most central collisions, beam energies from -10 to -150 MeV/nucleon can result in the formation of single nuclear systems with excitation energies from several to tens of MeV/nucleon. In such a range of excitation energies, previous experiments have indicated possible transitions between sequential binary (SB) disassembly mechanisms and multifragmentation (MF) (see Ref. 1 for a recent review). Detailed theoretical calculations[2-5] have predicted that the equivalent of a proper liquid-gas phase

+Invited talk, 10^{th} Winter Workshop on Nuclear Dynamics, Snowbird, Utah (Jan. 15-21, 1994).

§National Superconducting Cyclotron Laboratory, Michigan State University; Department of Chemistry, State University of New York - Stony Brook; Department of Physics, U. of Michigan - Dearborn; Cyclotron Institute, Texas A&M University; Department of Physics and Astronomy, U. of Iowa.

transition in finite nuclear systems occurs at excitation energies on the order of 10 MeV/nucleon for systems of mass ~100. The possibility that transitions in disassembly mode from SB to MF are an artifact of such a liquid-gas phase transition is, however, only one of many. Systematic experimental studies of the system mass and excitation energy dependence of the predominant disassembly mechanisms and the applicability of the various theoretical descriptions are therefore necessary. In this contribution, such studies based on event shape analyses of a comprehensive set of experimental data are described.

The experimental data was collected using the MSU 4π Array[6] at the National Superconducting Cyclotron Laboratory. Reactions in the entrance channels $^{12}C+^{12}C$, $^{20}Ne+^{27}Al$, $^{40}Ar+^{45}Sc$, $^{84}Kr+^{93}Nb$, and $^{129}Xe+^{139}La$ were measured with a minimum bias trigger in 5-10 MeV/nucleon steps in beam energy, up the maximum energy available from the K1200 Cyclotron for each projectile: 155, 140, 115, 75, and 60 MeV/nucleon, respectively. A detailed description of the data collection can be found in Ref. 7.

The analyses of these data will proceed via the study of the average event shapes, which summarize aspects of the three-dimensional average patterns of the particle emission as viewed from the center of momentum (CM) frame. The cartesian components of the CM frame particle momenta, $p^{(k)}$, are used to fill a tensor,[9] $F_{ij} = \sum_k^N [p_i^{(k)} p_j^{(k)} / 2m_k]$, in each event. The normalization of the eigenvalues of this tensor, t_i, via $q_i = t_i^2 / \sum_{i=1}^3 t_i^2$, allows the calculation of the sphericity[8] using $S = \frac{3}{2}(1 - q_3)$, where q_3 is the largest normalized eigenvalue. All shape observables extracted from F_{ij}, e.g. S, depend strongly[12] on the number of particles, N, included in the sum in F_{ij}. For a given value of N, particle emission patterns that are isotropic in a momentum space coordinate system that spatially coincides with the CM frame have the largest possible sphericities, while otherwise deformed emission patterns have smaller sphericities.

Given methods to remove the dependence of S on N, it is possible to extract information concerning the impact parameter and the characteristics of the predominant reaction mechanisms from shape analyses. The sensitivity of the sphericity to the impact parameter is provided by the increasing probability for the emission of particles from spectator-like sources as the impact parameter is increased. Particles emitted from such sources have relatively large momenta and forward/backward focussed emission angles when viewed from the CM frame, and hence strongly suppress the sphericity. Also, in the most central collisions, SB disassembly of the system at rest in the CM frame results in emission patterns that are more elongated in momentum space than those expected for MF reactions.[8,11] The finite values of the multiplicities, N, and inefficiencies in the central event selection conspire to suppress $\langle S \rangle$, and to decrease the distinctions in average shape between SB and MF events.

2. The Selection of Central Events

The selection of the most central experimental collisions constrains the mass of

the excited nuclear system via the projectile and target masses and results in a monotonic relationship between the beam energy and the excitation energy in this system. Software cuts on global observables, i.e. centrality variables, that are assumed to be correlated with the impact parameter are used to select samples of the most central events. One must ensure, however, that the specific cut used to select these events is relatively inefficient at selecting larger impact parameter events with significant topological fluctuations, and does not autocorrelate with subsequent stages of the analysis.

The relative efficiencies of various cuts for small impact parameter events were evaluated under the assumption that particle emission from projectile and target-like sources severely elongates that shape of the event in the CM frame.[10] For each entrance channel and beam energy, five different samples of events were produced for which the value of a given centrality variable was in the maximal ~10% of it's minimum bias spectrum. For the actual thresholds placed on the different centrality variables for this study (see Ref. 13), impact parameters $\langle b \rangle / [R_P + R_T] \sim 0.26$–$0.32$ are expected in each sample from (approximate) geometrical arguments. In each sample separately, the average sphericity $\langle S \rangle$ versus the total charged particle multiplicity was extracted. At a specific total charged particle multiplicity in these samples of selected events, the most(least) efficient small impact parameter cut is assumed to result in the largest(smallest) $\langle S \rangle$.

To more clearly depict the relative efficiencies of different centrality variables studied with these data, these average sphericities are "reduced" in a way that preserves the insensitivity of the present comparisons to the finite multiplicity distortions. At each total charged particle multiplicity, the values of $\langle S \rangle$ are divided by the semi-inclusive average sphericities, $\langle S_{inc} \rangle$, which are obtained for each entrance channel, beam energy, and multiplicity without a centrality cut. These ratios are then averaged over the multiplicity in each sample of selected events, using weights for each multiplicity obtained from the number of counts in each bin.

These "multiplicity-averaged reduced (central) event-averaged sphericities" are shown versus the beam energy for all five entrance channels in Figure 1. The centrality variables compared are the total charged particle multiplicity, N_{chgd} (solid), the total proton multiplicity, N_p (long dashed), the total charge of hydrogen and helium isotopes, Z_{LCP} (dot dashed), the total charge in a software gate centered at mid-rapidity, Z_{MR} (short dashed), and the total transverse kinetic energy, KE_T (dotted). The variables Z_{MR} and KE_T are defined as described in Ref. 14.

In the two lightest entrance channels, ^{12}C+^{12}C and ^{20}Ne+^{27}Al, centrality cuts on the variables KE_T and N_p lead to the largest average reduced sphericities, and hence are thus the most efficient for the selection of small impact parameters in these reactions. The results for the ^{40}Ar+^{45}Sc reactions are similar to those from the ^{12}C+^{12}C and ^{20}Ne+^{27}Al reactions for the same range of beam energies. However, for ^{40}Ar+^{45}Sc reactions at beam energies below about 45 MeV/nucleon, small impact parameter cuts based on the multiplicities of light particles, i.e. on Z_{LCP} and N_p,

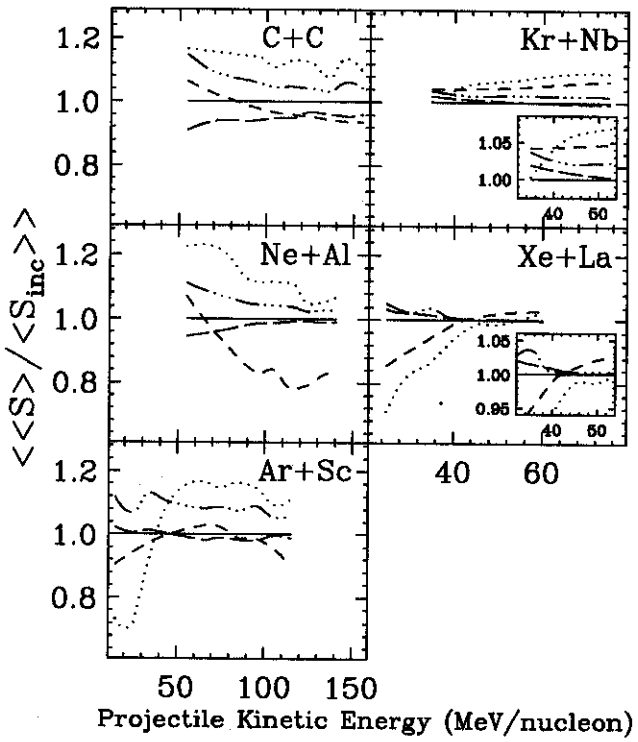

Fig. 1: The average reduced sphericity versus the beam energy for separate samples of events passing ~10% cuts on the different centrality variables listed in the text.

are apparently the most efficient. These light particle multiplicity variables are also the most efficient for beam energies below ~40 MeV/nucleon in the ^{129}Xe+^{139}La entrance channel. In the ^{84}Kr+^{93}Nb and ^{129}Xe+^{139}La reactions above about ~45 MeV/nucleon, the most efficient centrality variables are KE_T and Z_{MR}, although the efficiencies of all of the centrality variables compared in Figure 1 become similar for increasing entrance channel mass.

The wiggles in these lines are related to that noted in Ref. 13. Autocorrelations between the average sphericity and the different centrality variables were checked via the study of $\Delta S = \sqrt{\langle S^2 \rangle - \langle S \rangle^2}$ in the different samples of selected events. If, at a specific multiplicity, an increasingly strict cut results in an increasing suppression of the width ΔS, it is assumed that a significant autocorrelation biases the observed values of $\langle S \rangle$ in the events selected by that cut. Significant suppressions of these widths relative to that obtained with lower thresholds on each centrality variable were observed for cuts generally stricter than ~1–3%, and were negligible for the ~10% cuts[13] used herein.

The beam energy-dependent transitions in the most efficient means of selecting the central events seen in Figure 1 are assumed to be related to similarly beam energy-dependent transitions in the predominant reaction mechanisms at these impact parameters. Copious light particle emission is expected from excited systems decaying by a sequential binary mechanism, due to the importance of the Coulomb and angular

momentum barriers during such decays. Thus, the most central collisions for an entrance channel and beam energy for which SB disassembly dominates would be those for which the largest light particle multiplicities were observed. The extent to which the transitions apparent in Figure 1 are an artifact of transitions from SB to MF disassembly in the small impact parameter collisions is further investigated in the following Sections. Events were generated using SB and MF model codes and an accurate software replica of the apparatus, and direct comparisons to the experimental central events were made.

In order to limit the selection of larger impact parameter collisions with significant topological fluctuations, a two-dimensional centrality cut will be used for all that follows. For each entrance channel and beam energy, this cut selects events in which the two most efficient centrality variables (from Fig. 1) exceeded the $\sim$10% thresholds[13] used above. This generally allowed $\sim$4–8% of the minimum bias events ($\langle b \rangle / [R_P + R_T] \sim 0.2$–$0.28$ geometrically). The comparisons to software events described in the next Section will also provide a means of evaluating whether $\langle b \rangle / [R_P + R_T]$ is really in the range 0.2–0.28 in the selected events.

3. Comparisons to Model Code Events

In this Section, events generated by a number of different model codes which embody either SB or MF disassembly are filtered through an detailed software replica of the MSU 4π Array and compared directly to the data. The event generation was performed in both dynamic (FREESCO[8]) and hybrid approaches, for which BUU[16] and QMD[17] calculations were used to describe the initial stages of the reactions. The "after-burners" used in the hybrid event generation were the Berlin[18] and Copenhagen[2,19] MF codes, as well as the SB codes GEMINI[20] and SEQUENTIAL.[21]

All of these codes were run with the default parameters with the exception of the charge, mass, and excitation energy in the composite system, which was extracted from the BUU calculations in the same manner as described in Ref. 22. A soft equation of state was assumed, and the calculations were terminated when the radial density profile of the composite system most closely resembled that of a ground state nucleus.[16] The Berlin and GEMINI codes also require a cut-off angular momentum, which was taken as the maximum angular momentum that can be supported by the predicted composite system formed for each entrance channel and beam energy.

According to the BUU and QMD calculations for the impact parameters predicted geometrically for the present two-dimensional cuts, some fraction of the nucleons in the entrance channel are not found in an excited residue at rest in the CM frame. In the present event generation, these particles are thermally emitted from projectile and target-like sources, using reasonable assumptions for the velocities and temperatures of these spectator-like sources for each reaction.

For a given excited nucleus and at a specific final state multiplicity, the values of $\langle S \rangle$ for the events generated using the SEQUENTIAL(Berlin) code should agree with those from the GEMINI(Copenhagen) codes, and this was found to be true to about the

~10% level. Thus, for clarity in the Figures below, only the results using the MF code Berlin[18] and SB code SEQUENTIAL[21] will be plotted. The average sphericities from the dynamic MF model FREESCO, and the hybrid MF models QMD+Copenhagen, and BUU+Copenhagen also agree to within ~10% at specific multiplicities, implying a relative insensitivity of the present shape comparisons to the method chosen for the specification of the input parameters to the decay codes. By assumption, the average shapes of the selected experimental events cannot be below the predictions of the SB model calculations, or above the predictions of the MF models.

The average sphericities of the central experimental(generated) events are plotted versus the measured(filtered) total charged particle multiplicity in Figure 2 for the ^{40}Ar+^{45}Sc and ^{129}Xe+^{139}La reactions. The crossed points are the results from the central experimental events, while the solid(dashed) lines are the results from the filtered BUU+MF(BUU+SB) events.

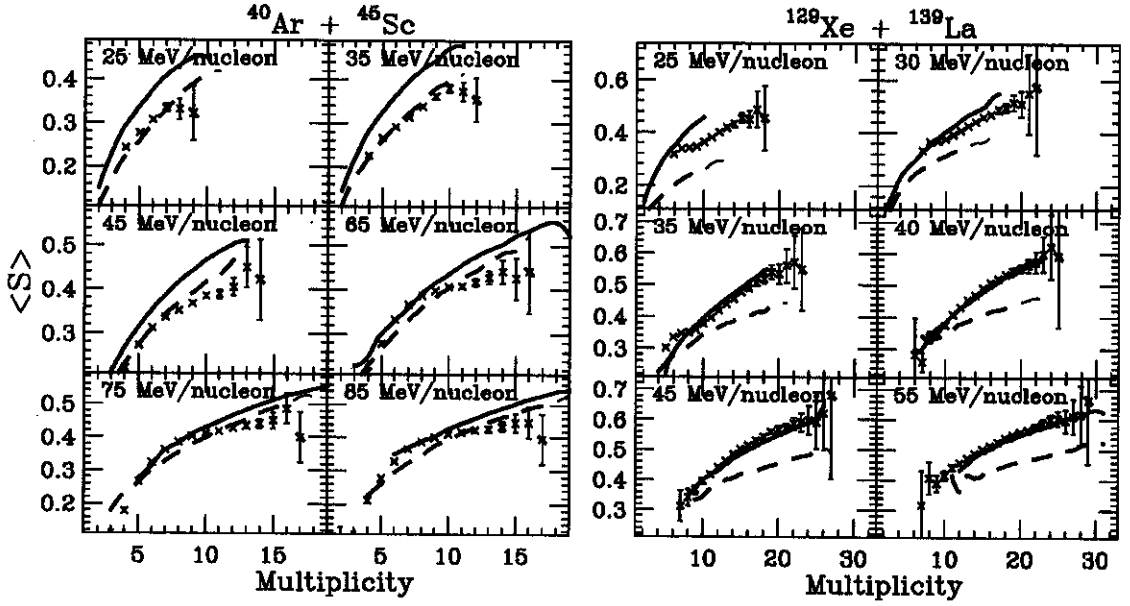

Fig. 2: The average sphericity versus the total charged particle multiplicity for the central experimental events (crossed points), the filtered BUU+SB events (dotted lines), and the filtered BUU+MF events (solid lines), for ^{40}Ar+^{45}Sc and ^{129}Xe+^{139}La reactions at the noted beam energies.

The average sphericities of the central ^{40}Ar+^{45}Sc reactions at beam energies near and below 45 MeV/nucleon are in agreement with those predicted by the BUU+SB codes. The data jump from the BUU+SB to the BUU+MF predictions for multiplicities on the order of eight between the beam energies of 45 and 65 MeV/nucleon. At larger multiplicities in this entrance channel, a dramatic suppression to below the SB model predictions is visible. This implies a failure in one or more of the assumptions used in the event generation described above, and is further investigated in the next Section.

In the central ^{129}Xe+^{139}La reactions, the average sphericities from the data are between the predictions of the filtered SB and MF models for all available beam

energies. The average sphericities increase, relative to the SB predictions, with the beam energy up to ~40 MeV/nucleon, above which they are in agreement with the MF model predictions.

4. Subset Shapes

The previous Section noted that the average sphericities of the largest multiplicity central events in the ^{40}Ar+^{45}Sc (and lighter) reactions were significantly below the predictions of the SB model calculations. In this Section, the sphericity of particular subsets of an event, i.e. the IMFs, will be distinguished from the sphericity of all of the particles in this event.

For all of the available entrance channels and beam energies, the largest average multiplicities of IMFs are found in the events with the largest total charged particle multiplicities. This is depicted in Figure 3, where each point style corresponds to a

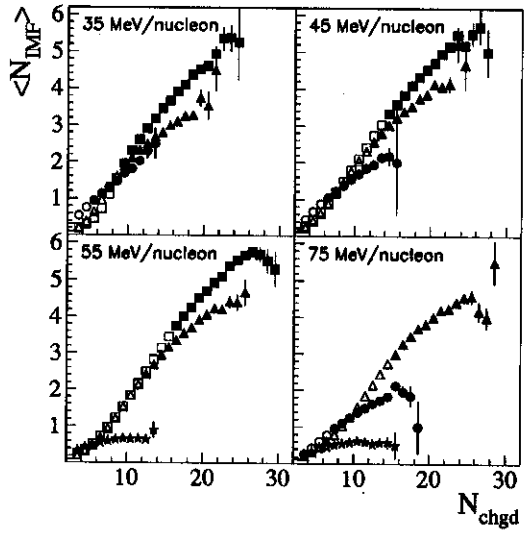

Fig. 3: The average number of IMFs versus the total charged particle multiplicity for ^{20}Ne+^{27}Al (stars), ^{40}Ar+^{45}Sc (circles), ^{84}Kr+^{93}Nb (triangles), and ^{129}Xe+^{139}La (squares) reactions at four representative beam energies. The N_{chgd} values above a threshold set for each system and beam energy allowing the maximal ~10% of the events are depicted with the solid points.

particular entrance channel. The solid points for each system and beam energy are those above a ~10% cut[13] on the inclusive spectrum of N_{chgd}. These solid points give a rough indication of the IMF multiplicities in samples of events of similar centrality for the different entrance channels and beam energies shown. A roughly universal dependence of $\langle N_{IMF} \rangle$ on N_{chgd} is noted for the more peripheral collisions (open points).

As depicted in Figure 4, the average IMF sphericities, $\langle S_{IMF} \rangle$, are generally well below the those predicted by the filtered SB model calculations for all IMF multiplicities. As the emission of IMFs is the most important at the largest charged particle multiplicities (Fig. 3), these suppressed IMF sphericities effect the suppression noted

in Fig. 2. A similar suppression of the IMF sphericities to below the SB model predictions was also observed for the central $^{12}C+^{12}C$ and $^{20}Ne+^{27}Al$ reactions.

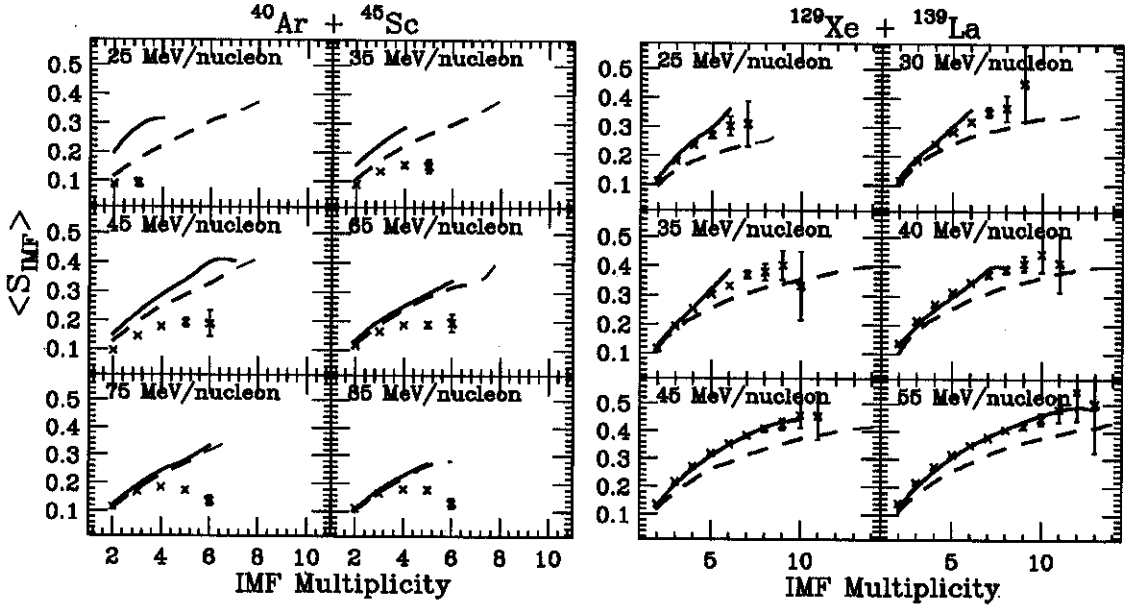

Fig. 4: The average IMF sphericity versus the IMF multiplicity for the central experimental events (crossed points), the filtered SB events (dotted lines), and the filtered MF events (solid lines), for $^{40}Ar+^{45}Sc$ and $^{129}Xe+^{139}La$ reactions at the noted beam energies.

For the central $^{129}Xe+^{139}La$ reactions, the average IMF sphericities are always between the SB and MF model predictions. Good agreement between the experimental IMF shapes and the MF model predictions are observed for beam energies above ~40 MeV/nucleon.

The IMF emission patterns in the $^{40}Ar+^{45}Sc$ entrance channel are far more deformed than that expected from the SB (or MF) model calculations. It is possible to imagine several possible causes for this effect. The first concerns impact parameter fluctuations. In the lightest entrance channels, there is simply not much information available upon which to base a centrality cut. An (integer) centrality variable's bin-width may be a significant fraction of the maximum value in the spectrum populated by the minimum bias events. As noted in Ref. 14, this leads to relatively larger fluctuations in the impact parameters deduced for each event. If this were the only possibility, a breakdown in the geometrical assumption that the maximal 4–8% of the minimum bias events corresponds to $\langle b \rangle / [R_P + R_T] \sim 0.2$–$0.28$ in the light entrance channels would be evident. The second possibility assumes that fluctuations in the initial stages of the reactions increase in importance as the entrance channel mass is decreased. In those collisions for which the equilibration of the excited system at mid-rapidity is particularly incomplete, some knowledge of the initial trajectories of the projectile and target nuclei could be retained by the particles in the final state. Prolate shapes oriented along the beam direction would be expected for such events, in similarity to that expected given significant contaminations to the samples

of selected central events from more peripheral collisions. The third possibility assumes the formation of non-compact geometries other than bubbles, e.g. toroids,[24] at freeze-out. These result in coplanar IMF emission patterns with the IMF flow angles $\theta_2 = \cos^{-1}(\mathbf{t}_2 \cdot \hat{\mathbf{z}})$ and $\theta_3 = \cos^{-1}(\mathbf{t}_3 \cdot \hat{\mathbf{z}})$ near 90°, where $\hat{\mathbf{z}}$ is the incident beam axis and $\mathbf{t}_2(\mathbf{t}_3)$ is the IMF eigenvector corresponding to the second largest(largest) eigenvalue.

Other aspects of the average shapes of the IMFs in the central events were studied to investigate these possibilities. The IMF shapes in the selected ^{40}Ar+^{45}Sc events (and in the lighter entrance channels) are manifestly prolate. For all values of N_{IMF}, the central event averaged probability that $t_3 - t_2 > t_2 - t_1$, corresponding to prolate IMF emission patterns, increases significantly for decreasing entrance channel mass. The CM frame ratios $\langle KE \rangle / 1.5 \langle KE_T \rangle$, calculated for each particle species in the selected events, also increase in this way. These observations point to an increase in the probability that the IMF emission patterns are elongated along the beam direction as the entrance channel mass is decreased, despite the event selection described in Section 2. To search specifically for toroidal IMF freeze-out configurations, the average IMF coplanarity, $C_{IMF} = \frac{\sqrt{3}}{2}(q_2 - q_1)$, and flatness $F_{IMF} = \frac{\sqrt{3}}{2}(t_2 - t_1)/(\sum_{i=1}^{3} t_i)$, were studied versus the IMF flow angle, θ_3, and the sum $\theta_3 + \theta_2$ for specific values of N_{IMF}. The average charge of the IMFs, the dispersion of the IMF charges, and the average IMF kinetic energy was plotted versus the values of the IMF flow angles and the shape observables C_{IMF} and F_{IMF}. No strong signal for toroidal geometries was seen using these observables, although these observables are, like S, strongly affected by the finite multiplicity distortions. Further analyses along these lines are presently underway.

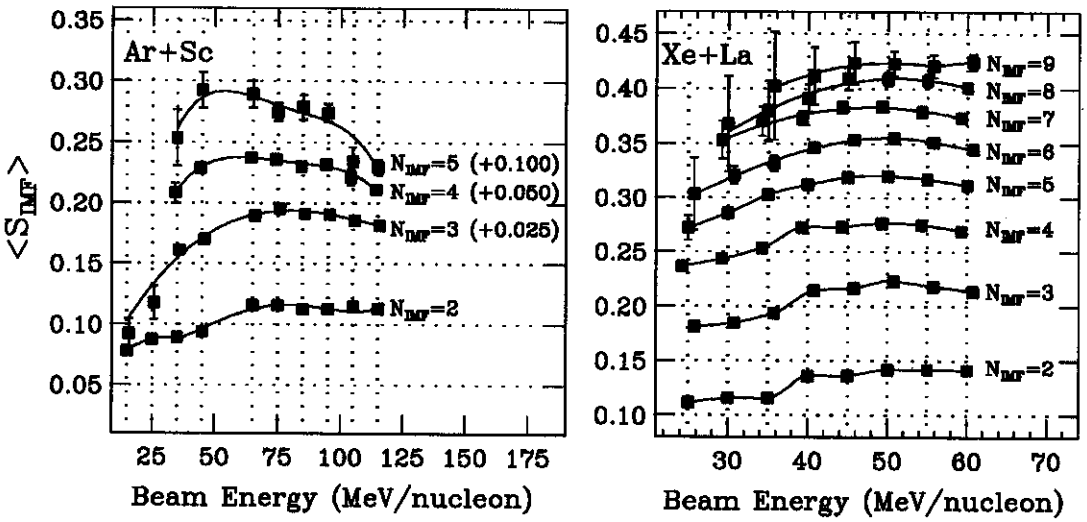

Fig. 5: The average IMF sphericity versus the beam energy for specific IMF multiplicities in central ^{40}Ar+^{45}Sc and ^{129}Xe+^{139}La reactions.

The beam energy dependence of the average IMF sphericities are shown in Figure 5 for specific IMF multiplicities in the central ^{40}Ar+^{45}Sc and ^{129}Xe+^{139}La reactions. Some points in Figure 5 have been vertically offset by the amounts shown for clarity,

while the solid lines are included only to guide the eye.

In the central ^{40}Ar+^{45}Sc reactions, a significant increase in the average IMF sphericities is observed at beam energies near 55 MeV/nucleon for all IMF multiplicities. A similar increase of the IMF sphericities is also observed in the central ^{129}Xe+^{139}La reactions at beam energies near 40 MeV/nucleon. In the ^{84}Kr+^{93}Nb entrance channel, the average IMF sphericity for each value of N_{IMF} increases by ~10–25% when going from 35 to 45 MeV/nucleon in beam energy, and is constant (to <5%) from 45 to 75 MeV/nucleon. Similar, although less pronounced, maxima in the average sphericities of all of the particles in the selected events are also observed near the beam energies that lead to maximal IMF sphericities.

5. Conclusions

The beam energy dependence of various projections of the shapes of the small impact parameter events in the available ^{40}Ar+^{45}Sc and ^{129}Xe+^{139}La reactions indicated critical phenomena at beam energies near 55±10, and 40±10 MeV/nucleon, respectively. The definition of a critical beam energy in the central ^{84}Kr+^{93}Nb reactions is made difficult by the lack of beam energies below 35 MeV/nucleon for this entrance channel. However, there are indications that MF disassembly dominates in the central ^{84}Kr+^{93}Nb reactions for beam energies near and above 45 MeV/nucleon. No critical behavior was observed in the central ^{12}C+^{12}C(^{20}Ne+^{27}Al) reactions for beam energies from 55 to 155(140) MeV/nucleon.

The beam energies at which the various analyses described above indicated critical phenomena in the central events in each entrance channel are depicted in Figure 6. Also included in this Figure is the critical beam energy observed by Cebra *et al.* for central ^{40}Ar+^{51}V reactions,[21] and the critical beam energies observed in a charge correlations analysis of the present data.[23] In this analysis, a clear transition in the relative sizes of the three largest fragments in central events is observed at beam energies of 47±10, 35±10, and 32±5 MeV/nucleon in the ^{40}Ar+^{45}Sc, ^{84}Kr+^{93}Nb, and ^{129}Xe+^{139}La entrance channels, respectively.

The various analyses indicate similar critical beam energies for each entrance channel. The transitional beam energies observed for the central ^{40}Ar+^{45}Sc reactions are significantly larger than those observed for the central ^{84}Kr+^{93}Nb and ^{129}Xe+^{139}La reactions.

The most obvious possibilities for this trend concern the open questions raised in Sections 3 and 4. These would involve an increasing importance of fluctuations in impact parameter, or in the degree of equilibration of the excited systems formed at one impact parameter, for decreasing entrance channel mass. Two other possibilities are noted, which should not, however, be considered until the two above have been fully explored. The third assumes an increase in the importance of quantum mechanical finite-size effects for the excited systems formed in increasingly lighter entrance channels. The fourth involves the fact that increasingly heavier entrance channels result in excited systems that are increasingly more proton-rich.

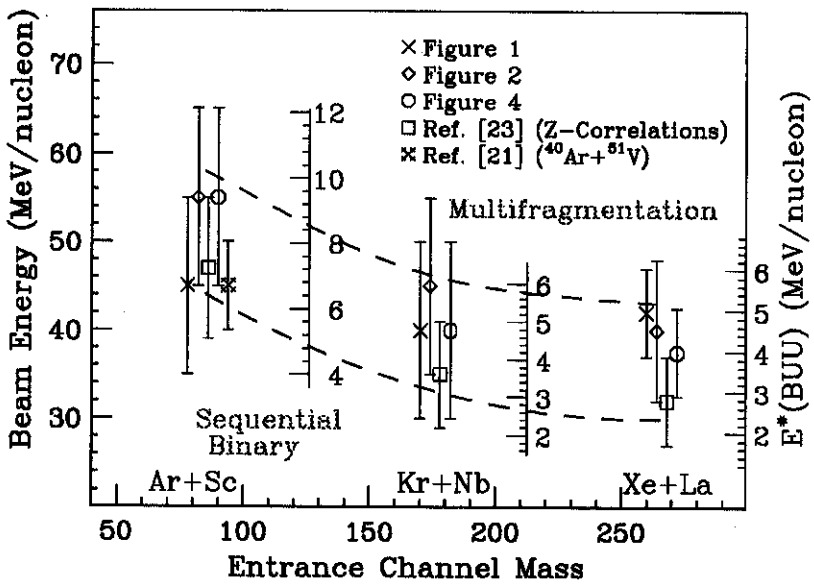

Fig. 6: A summary of the results of the present shape analyses indicating transitions in various characteristics of the predominant reaction mechanisms for the systems formed in the central collisions in the different entrance channels. Predictions of the BUU calculations for the approximate excitation energies reached in the selected events are given for each entrance channel on the right side axes. The dashed lines are included only to guide the eye.

The investigation of these open questions is possible only after the remeasurement of these reactions with an improved experimental acceptance. More efficient impact parameter selection and studies of the characteristics of pre-equilibrium particle emission would then be possible. A more sensitive search for non-compact geometries would be feasible. Larger total event and subset multiplicities would be available for event shape analyses. Recently, important upgrades to the MSU 4π Array were finished, which dramatically improve the forward acceptance and substantially lower the overall particle kinetic energy thresholds. The entrance channels ^{40}Ar+^{45}Sc, ^{129}Xe+^{139}La, and ^{197}Au+^{197}Au were recently (re)measured with the improved apparatus, each for a systematic set of beam energies, while systematic experiments in the entrance channels ^{28}Si+^{27}Al, ^{58}Ni+^{58}Ni, and ^{84}Kr+^{93}Nb are scheduled.

6. Acknowledgements

We gratefully acknowledge helpful discussions with P. Danielewicz, L. Phair, W. Bauer, and J. Krieger. This work was supported by the U.S. National Science Foundation under Grants No. PHY 89-13815 and No. PHY 92-14992.

7. References

[1] L.G. Moretto and G.J. Wozniak, *Ann. Rev. Nucl. Part. Sci.* (May, 1993).

[2] J.P. Bondorf *et al.*, *Nucl. Phys.* **A448**, 753 (1986), and references therein.

[3] D.H.E. Gross, *Prog. Part. Nucl. Phys.* **30**, 155 (1993), and references therein.

[4] A.S. Botvina *et al.*, *Nucl. Phys.* **A475**, 663 (1987).

[5] W. Bauer, *Phys. Rev. C* **38**, 1297 (1988).

[6] G.D. Westfall *et al.*, *Nucl. Inst. and Methods* **A238**, 347 (1985).

[7] G.D. Westfall *et al.*, "Advances in Nuclear Dynamics, Proc. of the 8^{th} Winter Workshop on Nuclear Dynamics", eds.: W. Bauer and B. Back, Jackson Hole, Wyoming (1992);
G.D. Westfall *et al.*, *Phys. Rev. Lett.* **71**, 1986 (1993);
E. Bauge *et al.*, *Phys. Rev. Lett.* **70**, 3705 (1993);
R.A. Lacey *et al.*, *Phys. Rev. Lett.* **70**, 1224 (1993).

[8] G. Fái and J. Randrup, *Nucl. Phys.* **A404**, 551 (1983).

[9] M. Gyulassy, K.A. Frankel, and H. Stöcker, *Phys. Lett.* **110B**, 185 (1982).

[10] H. Stöcker *et al.*, *Nucl. Phys.* **A387**, 205c (1982).

[11] J. A. López and J. Randrup, *Nucl. Phys.* **A491**, 477 (1989).

[12] P. Danielewicz and M. Gyulassy, *Phys. Lett.* **129B**, 283 (1983);
J.P. Bondorf *et al.*, *Phys. Lett. B* **240**, 28 (1990).

[13] It is not always possible to select a specific fraction of the impact parameter inclusive events, as often the case for centrality variables that are integer quantities. The threshold on a centrality variable chosen was the lowest possible bin for which <10% of the minimum bias events are in and above this bin. Generally, 7–10% of the events are selected by these cuts.

[14] L. Phair *et al.*, *Nucl. Phys.* **A548**, 489 (1992).

[15] G. Fái *et al.*, *Nucl. Phys.* **A381**, 557 (1982).

[16] W.-Bauer and C.M. Mader, private communication;
C.M. Mader, Ph.D. Thesis, Michigan State University, unpublished (1993).

[17] G. Peilert, private communication;
J. Achelin *et al.*, *Phys. Rev. C* **37**, 2451 (1988).

[18] A.R. DeAngelis and D.H.E. Gross, private communication;
X.-Z. Zhang *et al.*, *Nucl. Phys.* **A461**, 668 (1987), and references therein.

[19] H.W. Barz *et al.*, *Phys. Lett. B* **267**, 317 (1991).

[20] R.J. Charity *et al.*, *Nucl. Phys.* **A483**, 371 (1988).

[21] D.A. Cebra *et al.*, *Phys. Rev. Lett.* **64**, 2246 (1990).

[22] D.R. Bowman *et al.*, *Phys. Rev. C* **46**, 1834 (1992).

[23] N. Stone, W.J. Llope, and G.D. Westfall, Preprint MSUCL-916, for submission.

[24] L.G. Moretto *et al.*, *Phys. Rev. Lett.* **69**, 1884 (1992);
W. Bauer, G.F. Bertsch, and H. Schulz, *ibid*, 1888 (1992).